Received: 24 May 2021 | Revised: 30 November 2021 | Accepted: 18 January 2022

DOI: 10.1002/tal.1926

RESEARCH ARTICLE

WILEY

A novel damped braced tube system for tall buildings in high seismic zones

Yoji Ishibashi[1] | Yuki Terazawa[2] | Haruki Tanaka[2] | Ryo Yokoyama[1] | Hiroki Mizuno[1] | Toru Takeuchi[2]

[1]Mitsubishi Jisho Sekkei Inc., Tokyo, Japan

[2]Tokyo Institute of Technology, Tokyo, Japan

Correspondence
Yuki Terazawa, Tokyo Institute of Technology, 4F-406, 2-12-1 Ookayama, Meguro-ku, Tokyo, Japan.
Email: terazawa.y.aa@m.titech.ac.jp

Funding information
Japanese Society of Seismic Isolation, Japan Society for the Promotion of Science Fellowships, Grant/Award Number: 21K14288

Summary

The damped outrigger system is known to efficiently provide additional damping in buildings with heights of over 250 m. However, particularly for supertall buildings in the center of Tokyo, Japan, the outrigger truss from the center core to the exterior columns need to span distances of more than 20 m. This increases the flexural stiffness demand on the outrigger that leads to larger truss depths making the damped outrigger system inefficient. For such tall buildings with large plans, a new damping modification system, the "damped braced tube system" is proposed, where the exterior surface of the elastic mega braces are partially removed vertically to create a split and are replaced with dissipaters (energy-dissipation devices). The damped braced tube system enhances the seismic performance as the exterior surfaces of the elastic mega braces work together with the damped slits like in a coupled wall system and increases the overall damping ratio. In this paper, numerical models were constructed based on a real project in Japan consisting of a 397-m supertall building employing the damped tubular braced system using oil dampers (referred to as viscous dissipaters). A series of generalized response spectrum based numerical analyses and optimizations were performed to minimize the seismic response. The proposed system exhibited improved damping performance with the first to third mode damping ratios reaching to more than 7% while providing a wide range of options for dissipater distribution for design. Finally, the elevation of the slit's base is recommended to be equal to 0.22 of the total building height considering the trade-off relationship between the first modal damping ratio and the fundamental period.

KEYWORDS
complex eigenvalue analysis, oil damper, response control, seismic optimization, supertall building

1 | INTRODUCTION

The number of buildings taller than 250 m has rapidly increased worldwide. According to the reference, while the number of buildings taller than 250 m built between 2000 and 2010 was only 66, the number of buildings built after 2010[1] increased to 470. However, in areas with a high seismic and wind hazard, the number of tall buildings is only 60 (about 10% of the 470) because expensive dissipaters are required to meet the large demands from the dynamic response. Nevertheless, about 50% of these 60 buildings have been constructed in only 3 years (2017 to 2020). These data suggest that the demand for tall buildings is accelerating due to the recent innovations in damping modification systems at high rate such

that it has outweighed the disadvantages of increased costs. Even in Tokyo (the capital of Japan), which is the most frequent seismic area all over the world, an approximately 400-m high supertall building is expected to be soon realized. Given that there are few supertall buildings in Japan, this project poses a huge challenge to design the first Japanese supertall buildings to withstand huge earthquakes.

The floor plan of tall buildings (especially multi-tenant office buildings) in Japan depends on its unique cultural and economic background of Japan. A typical office floor plan of a tall building in central Tokyo is shown in Figure 1. Integrated offices without partitions that a tenant owner may use flexibly are preferred in Japan. Specially, in Tokyo, where politics, economy, and population are densely concentrated in one place, developers prefer real estate that may maximize the leasable floor area because of the huge demand for floor space despite the high tenant rent. Therefore, for tall buildings in Tokyo, a floor plan with long spans of 18–20 m from the core, which is close to the evacuation planning limit, and an elevation with a small aspect ratio that improves the rentable ratio (= rentable area/total area) are typical. Furthermore, in Japan, there are no legal regulations on depth to span ratios considering natural lighting as it is not included in the scope of architectural planning of tall building. In this study, a numerical model with a plan size of 97.2 by 97.2 m and a building height of approximately 390 m considering an aspect ratio of about 4.08 is constructed based on the actual project[2] being planned in Tokyo. In the case of such a large plan, a square plan with a center core and a column-free space of about 20 m on all four sides provides the highest rentable ratio. However, a building with such a large floor area compared to its height is subject to large seismic forces. Furthermore, the fundamental period of this supertall building coincides with the predominant period range in the Tokyo region (7.0 to 9.0 s), as shown in Figure 6. Considering the huge fault running along the Nankai Trough where the peak spectral velocity S_v is 80 to 120 cm/s, a supertall building in Tokyo is required to exhibit extremely high seismic performance compared to other regions, and therefore, it is crucial to adopt a powerful damping modification system.

The damped outrigger system[3] has been adopted in areas of high seismic and wind hazards as a damping modification system for tall to supertall buildings. In a damped outrigger system, energy-dissipation devices (hereafter dissipaters) are inserted between the outrigger trusses and exterior columns and, the dissipater efficiently absorbs seismic and wind energy by deforming vertically. The structure may obtain high additional damping performance while the column-restrained outrigger truss bends back the center core as in a conventional outrigger system.[4] Its excellent seismic performance and optimum outrigger height have been confirmed numerically and experimentally in the existing research.[3–9] However, the damping performance of the damped outrigger system depends on the flexural stiffness of the outrigger truss, and a large depth of the outrigger truss is often required to obtain the best damping performance.[9] The flexural stiffness of the outrigger truss, which is equal to that of the fixed supported cantilever beam, is inversely proportional to the cube of the outrigger truss's span. In this project, the span from the center core to the exterior column is 20 m, and the flexural stiffness of the outrigger truss is thus reduced to about 20% from that of a typical outrigger system with a span of about 12 m (typical in European countries). A preliminary design option of a damped outrigger system with nonlinear oil dampers adopted in the project is shown in Figure 2. In this study, the Japanese structural analysis software RESP[10] was used for the nonlinear response history analysis by the Newmark β numerical time integration method. The nonlinear oil damper was modeled as a Maxwell model composed of a dashpot having the material nonlinearity as shown in Figure 7 and a spring. The corresponding material parameters of viscous coefficient C_d, spring stiffness K_d and relief velocity V_R were set as 235 kN·s/mm, 1650 kN/mm, and 31 mm/s. As shown in Figure 2, the damped

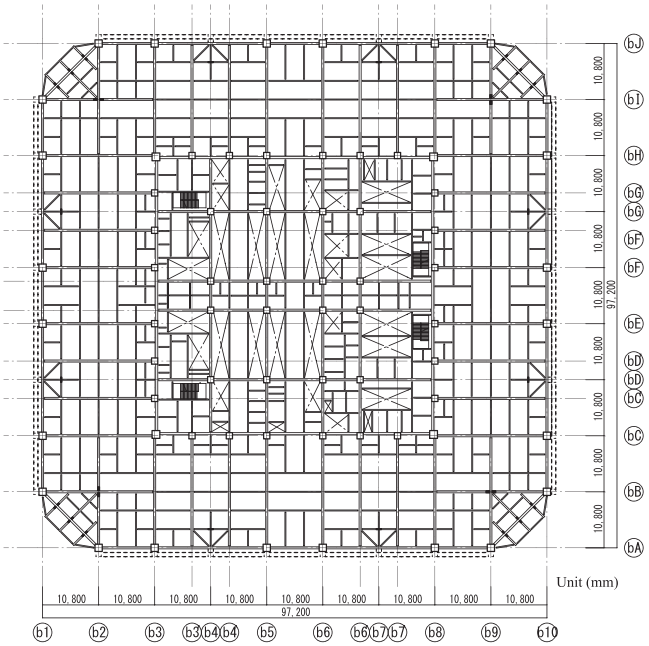

FIGURE 1 Typical floor plan of a tall building in Tokyo

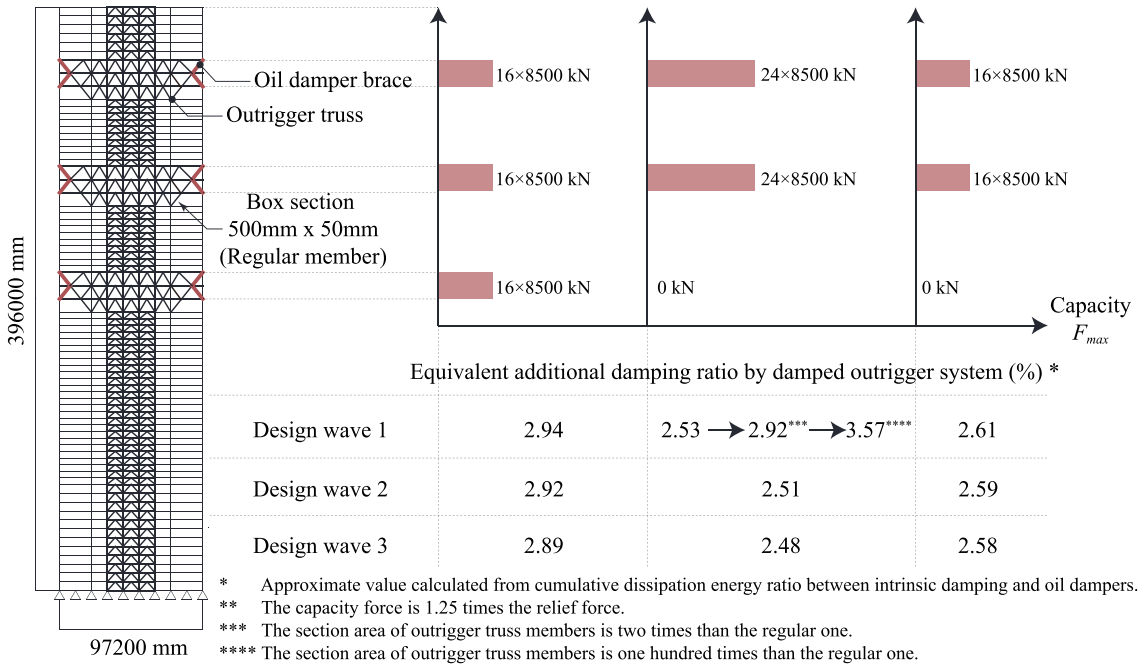

Equivalent additional damping ratio by damped outrigger system (%) *

Design wave 1	2.94	2.53 → 2.92*** → 3.57****	2.61
Design wave 2	2.92	2.51	2.59
Design wave 3	2.89	2.48	2.58

* Approximate value calculated from cumulative dissipation energy ratio between intrinsic damping and oil dampers.
** The capacity force is 1.25 times the relief force.
*** The section area of outrigger truss members is two times than the regular one.
**** The section area of outrigger truss members is one hundred times than the regular one.

FIGURE 2 Damping performance of the damped outrigger system applied to the target building

outrigger system contributes to only 2.0% to 3.0% of the first modal damping ratio even if an unrealistic member with the section area set to 100 times that of the box section 500 × 50 mm is adopted in the truss member. This trial suggests that the damped outrigger system may not necessarily be efficient for a tall building with a large floor plan. A damped core system where shear dissipaters are distributed along the core is common in Japan (e.g., Shinjuku Center Buildings and Mode Gakuen Cocoon Tower[1]). However, the flexural response of the core is predominant in buildings over 300 m high, and therefore, the shear dissipaters may not absorb seismic energy efficiently, significantly decreasing the damping performance. Furthermore, the section design of the core also becomes more difficult due to the increased imposed demands. Therefore, there was a need to develop a strong and efficient damping modification system applicable even for a supertall building with a large floor plan.

This paper proposes a new damping modification system named as the damped braced tube system where the exterior surface of the elastic mega braces are partially removed vertically to create a split and are replaced with dissipater, as shown in Figure 3. In this study, viscous dissipaters like linear or nonlinear oil damper, and no buckling-restrained braces are adopted in the damped braced tube system. In a damped braced tube system, elastic mega braces are placed on the outer tube, and the exterior surface with the damped slit works like a coupled wall system, which increases the seismic performance (due to the shorter fundamental period if compared to a conventional braced tube system and a larger damping ratio due to the damped slits.) A few ("not all") elastic mega braces are replaced with oil dampers. The remaining elastic mega braces withstand the wind and seismic loading. A hybrid system composed of this damped braced tube system with nonlinear oil dampers, and a special moment-resisting frame is being applied to the actual project[2] in Tokyo. Note that the braced frame systems are sometimes classified as diagrid systems in Japan, and the damped braced tube system applied to this project is commercially called the "damped diagrid."

A system similar to the damped braced tube system is the mega brace dampers façade system applied to the 181 Fremont tower[11] although the damping mechanism differs from the latter. In the mega brace dampers façade system, the mega brace damper, which consists of a buckling-restraining brace and a fluid viscous damper brace in parallel, contributes to both the horizontal stiffening and damping of the building. However, in this building, fluid viscous dampers are designed to work only for small-amplitude vibration caused by wind loads and small earthquakes, and for large earthquakes corresponding to the maximum considered earthquake (MCE) level, buckling-restrained braces work only as fuses and therefore do not contribute to the damping.

The objective of this study is a numerical investigation and a demonstration of the seismic performance (i.e., the fundamental periods, the damping ratios, and the seismic response reduction effect) of the proposed damped braced tube system based on the real-life application to a supertall building. Optimal dissipater distributions to maximize the effects of the dissipaters are also studied. To achieve a good structural design of the damped braced tube system, the right balance between the reduction of the horizontal stiffness by the slit and the additional damping effect by the dampers is important. Therefore, complex eigenvalue analysis and response spectrum analysis were performed to investigate the exact modal characteristics considering the non-proportional damping from oil dampers. The relationship between the seismic performance and the design parameters (the size of the slit and the dissipater amount) is discussed based on the results of the parametric study and seismic optimization. Note that in this paper, the term "dissipaters" refers to viscous damping devices including oil dampers.

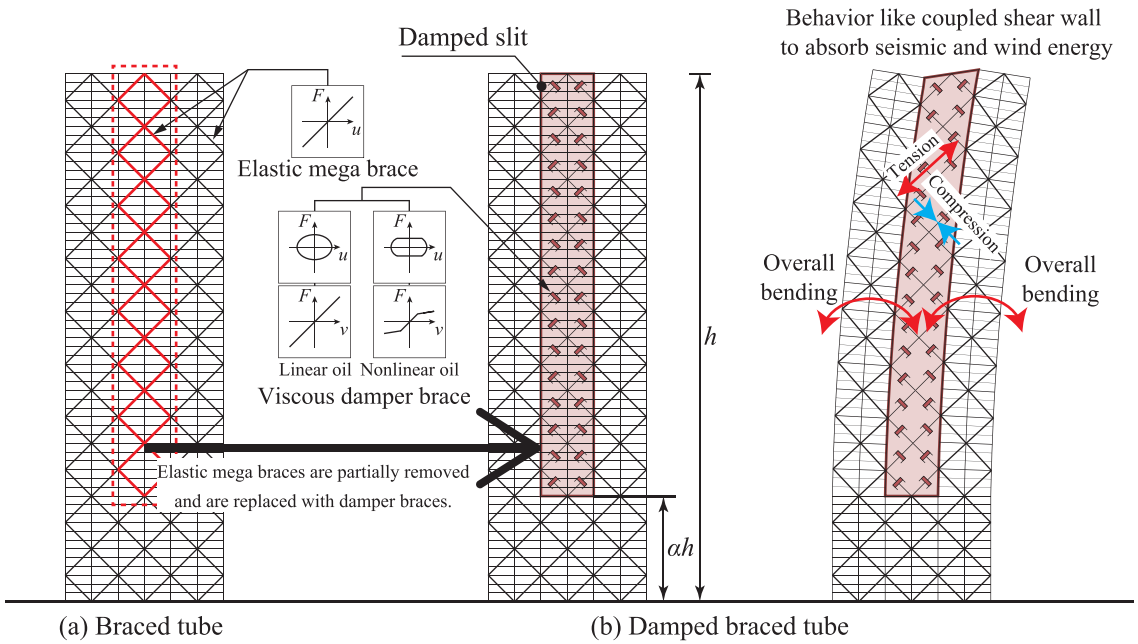

FIGURE 3 (a–c) Schematic diagram of damped braced tube system

2 | METHODOLOGY

2.1 | Numerical model and seismic input ground motions

The schematic image of the numerical model and the structural members are shown in Figure 4. This numerical model is a simplified form of the actual project, and only the superstructure from G. L was modeled. The actual floor plan is shown in Figure 1. The column of the braced tube spans a distance of about 10.8 m. The configuration of elastic mega braces is based on the actual architectural plan. The building structure weighs 1.66×10^6 kN, the floor weight is 3.78×10^6 kN, the exterior wall weight is 5.51×10^5 kN (3.58 kN/m^2) and the total seismic weight is 5.99×10^6 kN (63.2 kN/m^2.) The section properties of the CFT columns, wide flange girders and elastic mega braces are summarized in Figure 4. These sections were designed using the allowable strength design method based on the Japanese building code against a load combination of the dead load and the static seismic loads with a base shear to weight ratio (known as the base shear coefficient) of 0.3. The sections of elastic mega braces were specially designed to remain elastic even against MCE level earthquake. In the numerical model, the columns and girders are modeled as beam–column elements, and the elastic mega braces are modeled as truss elements. The girders are rigidly connected to the column. The nodes on the column bases are pin supported. A rigid diaphragm was assigned to each floor. This numerical model is labeled as the "No damper model," and the other models including the damped slits are labeled as the "Damped braced tube model." These stiffness elements remained elastic throughout the analyses. Referring to the actual project, only the elastic mega braces in the corner of the exterior surface were replaced with linear or nonlinear dampers (viscous dissipater), which acts as the damped slit, and most of the other elastic mega braces bear the seismic and wind loads. The linear and nonlinear oil damper were modeled as simple dashpots, and material nonlinearity (discussed later) shown in Figure 7 was assigned in the nonlinear oil damper. The modal characteristics of the representative examples of "No damper model" and "Damped braced tube models with linear or bilinear oil dampers" are shown in Figure 5. Thus, it may be concluded that an appropriately designed damped braced tube system may significantly increase the 1st to 4th modal damping ratios.

This section briefly reviews the Japanese lateral load demands. In Japan, the wind loads for tall buildings are determined by wind tunnel tests. The reference wind velocity is 34 m/s (at Tokyo) for 50-year return period and 43 m/s for 500-year return period. Service-level earthquake (SLE) and design-basis earthquake (DBE) earthquakes correspond to the Japanese Level-1 earthquake and Level-2 earthquake load, respectively. For tall buildings, the DBE level target design spectrum with a peak spectral acceleration of 0.8 g corresponding to a 473-year return period on the bedrock is used for nonlinear response history analysis and the structural members are permitted to yield. The SLE level target design spectrum adopts a peak spectral acceleration of 0.16 g (i.e., one fifth part of that of the DBE level) corresponding to a 43-year return period on the bedrock. The structural members are required to remain elastic, and the story drift demands are required to be less than 0.5% rad after an SLE level earthquake.

The acceleration and velocity response spectra of the input seismic waves are shown in Figure 6. The Japanese Building Standard Law[12] prescribes to use spectrally matched waves and site specific special waves including long period earthquakes for tall buildings using nonlinear

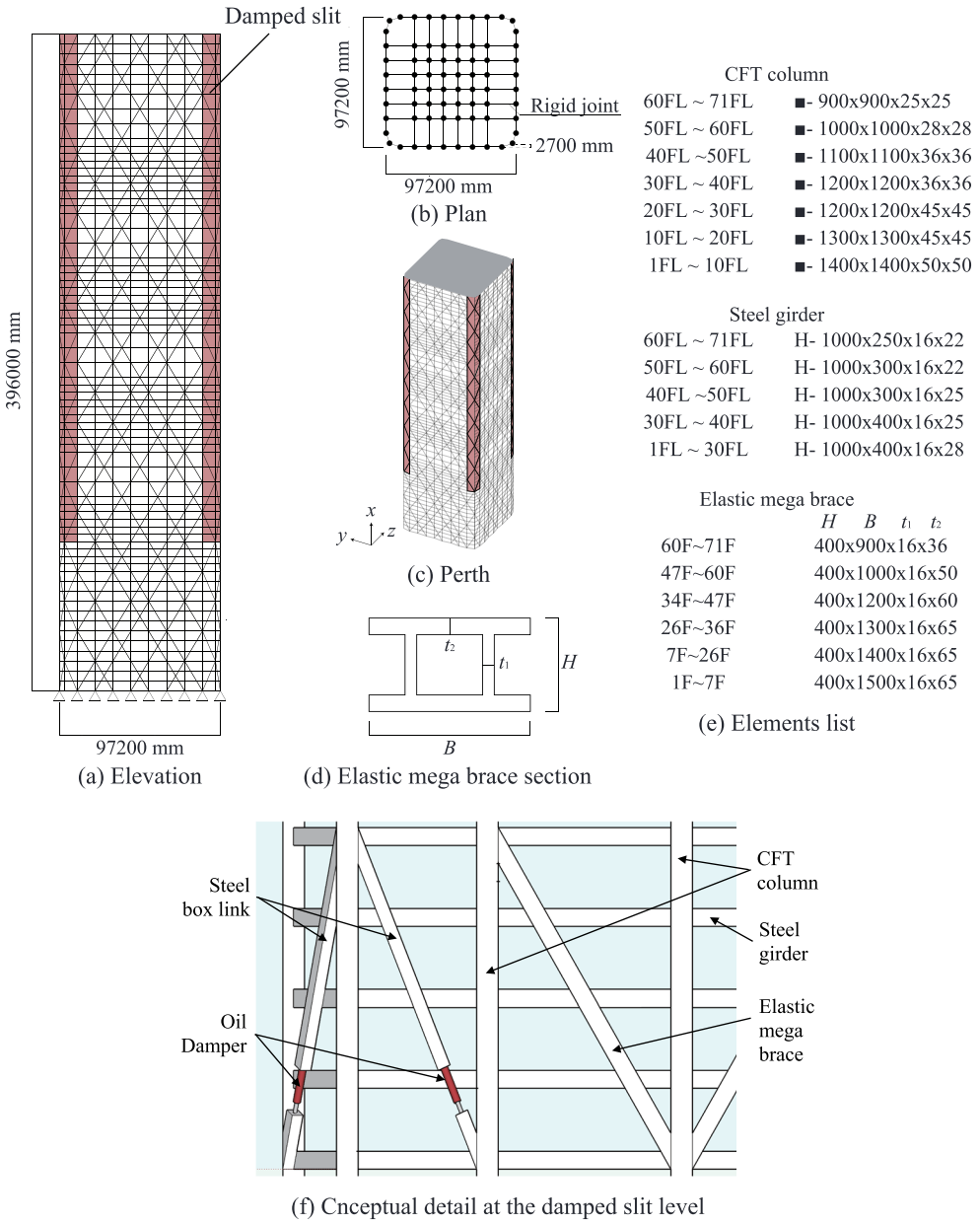

FIGURE 4 (a–f) Schematic image of the numerical model and member specifications

response history analysis procedure. El Centro, Taft, Hachinohe, and JMA-Kobe waves are typically selected for spectral matching. Following this Japanese design practice, in this study, the input ground motions consist of the above-mentioned spectrally matched waves and an artificial Nankai Trough seismic waves KA1[13] for tall buildings considering the soil structure of the Tokyo area. Please note the target period range for spectrally matching is 0.02 to 10.0 s for tall buildings, and a recorded motion is iteratively matched using Fourier and inverse Fourier transform until the response spectrum error converge based on the Ministry of Construction.[14] As shown in Figure 6, while KA1 mainly excites the first mode response, the spectrally matched waves excites not only the first mode response but also the higher mode responses.

2.2 | Numerical simulation method

The seismic performance (i.e., the fundamental periods, the damping ratios and the seismic responses) of damped braced tube system is evaluated by a generalized response spectrum analysis.[15–17] GRSA is a series of numerical analysis which iteratively performs complex eigenvalue analysis and response spectrum analysis, and is suitable for vast parametric studies and seismic optimizations[16] because GRSA may quickly evaluate the

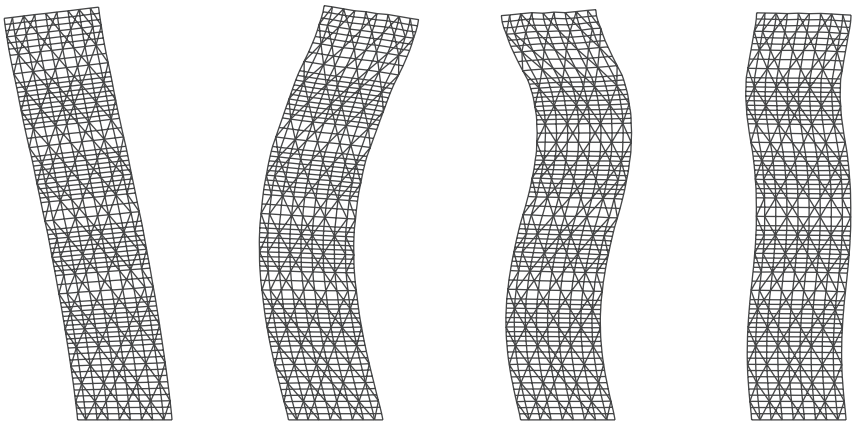

	1st mode	2nd mode	3rd mode	4th mode
(a) No damper model				
Natural period	6.43 s	2.20 s	1.25 s	0.89 s
Damping ratio	2.00 %	2.00 %	2.91 %	3.90 %
Effective mass ratio	59.3 %	16.2 %	4.80 %	1.06 %
(b) Damped braced tube model with linear oil dampers (uniform damper distribution) $\{\alpha, 8\{n_i\}^{\mathrm{T}}\{C_{di}\}\} = \{0.22, 20.0\ \mathrm{MNs/mm}\}$				
Natural period	8.07 s	2.42 s	1.33 s	0.94 s
Damping ratio	11.65 %	11.54 %	13.06 %	14.22 %
Effective mass ratio	65.1 %	16.5 %	5.43 %	2.85 %
(c) Damped braced tube model with nonlinear oil dampers (uniform damper distribution) $\{\alpha, 8\{n_i\}^{\mathrm{T}}\{C_{di}\}\} = \{0.22, 20.0\ \mathrm{MNs/mm}\}$				
Natural period	8.23 s	2.53 s	1.37 s	0.97 s
Damping ratio	8.51 %	10.07 %	11.21 %	11.63 %
Effective mass ratio	60.3 %	17.3 %	5.63 %	3.09 %

FIGURE 5 Fundamental periods and modal shapes of the "No damper model" and "Damped braced tube model"

seismic performance of a 3D model with finite dissipaters. In GRSA, the nonlinearity of dissipaters is simulated by the iterative computation of equivalent linearization approach, and the seismic response is evaluated using the complex modal characteristics of the vibration system with the equivalent linearized variables and the modified complete quadratic combination method (the modified CQC method) proposed by Sinha et al.,[18] as shown in Equation 1. Note that the elasto-plastic response of the main structure is not considered in the current GRSA.[17]

$$R_{\mathrm{CQC}} = \sqrt{\sum_{s=1}^{n}\sum_{r=1}^{n} B_s B_r S_{d_s}(\omega_s,\xi_s) S_{d_r}(\omega_r,\xi_r)\cos(\theta_s-\theta_r)\rho_{sr}} \tag{1}$$

where s and r are the modal numbers, n is the number of the selected modes for CQC, ξ is the modal damping ratio, ρ is the modal correlation coefficient of the conventional CQC, ω is the circular natural frequency, S_d is the displacement response spectrum value, $B = 2|\mathrm{Re}(\lambda^{*}\beta\phi)/\sin(\theta)|$, $\theta = \tan^{-1}[-\mathrm{Re}(\lambda^{*}\beta\phi)/\mathrm{Re}\,(\beta\phi)]$, λ is the complex eigenvalue, β is the complex participation factor, ϕ is the complex modal vector component, and * is the index of the complex conjugate.

In GRSA, the response spectrum values per 0.01 s and the initial damping ratio $\xi_0 = 1\%$, 2%, 3%, 5%, 10%, 15%, 20%, and 30% is given by the external datasets and then adjusted to the precise damping ratio ξ using the damping modification factor D_h calculated by Equation 2.

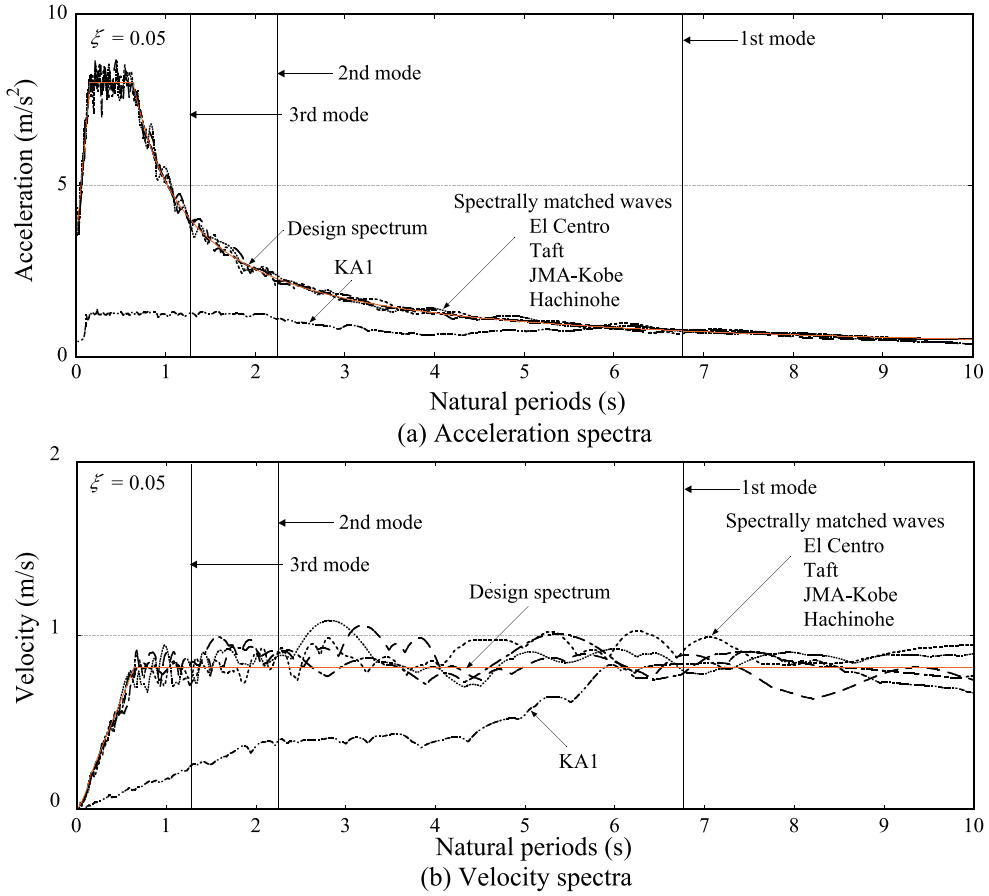

FIGURE 6 (a,b) Response spectra of the selected seismic inputs ground motions

$$D_h = \begin{cases} (D_{h0}-1)(5T)+1 (0 \le T < 0.2) \\ D_{h0} (0.2 \le T < 2.0) \\ D_{h0}\left\{\sqrt{\xi/\xi_0}(T-2)/40+1\right\} (2.0 \le T < 8.0) \end{cases} \quad (2)$$

where T is the fundamental period, $D_{h0} = \sqrt{(1+\alpha\xi 0)/(1+\alpha\xi)}$ and α is 75 for artificial waves.

The force–velocity relationship of nonlinear oil dampers is shown in Figure 7. The oil damper is a kind of viscous dissipater where the force is linearly proportional to the velocity. In the nonlinear oil damper, the viscous coefficient C_d is reduced by a relief mechanism to prevent the failure of the device when the relative velocity of the dissipater reaches the upper limit V_R. In GRSA, the equivalent viscous coefficient C_{deq} is iteratively calculated by Equation 3[19] based on equalizing the capacity of energy absorbed at the maximum velocity V_{max}, and is included in the damping matrix **C**.

$$C_{deq} = \left\{(p_d\mu_d - p_d + 1)^2 + p_d - 1\right\} C_d / (p_d {\mu_d}^2) \quad (3)$$

where p_d is the secant viscous coefficient ratio, C_d is the initial viscous coefficient, V_{max} is the combination response value by the modified CQC method, and μ_d is the relief ratio (V_{max}/V_R). In this paper, the nonlinear oil damper is modeled as a simple dashpot not considering the connection stiffness. V_R is 30 mm/s and p_d is 1.2%.

The 3D model has about 15,000° of freedom and requires approximately 50 MB of RAM to store the global system matrix including the mass, stiffness, and damping matrix as sparse matrix. Only one processor is assigned to one GRSA, and 56 GRSAs are performed on the campus supercomputer in parallel at the same time. One GRSA takes about 2 min for the damped braced tube with the linear oil dampers and takes about 10 min for the damped braced tube with the nonlinear oil dampers. Therefore, GRSA is suitable for extensive parametric studies to investigate the dynamic responses of structural systems with finite dissipaters.

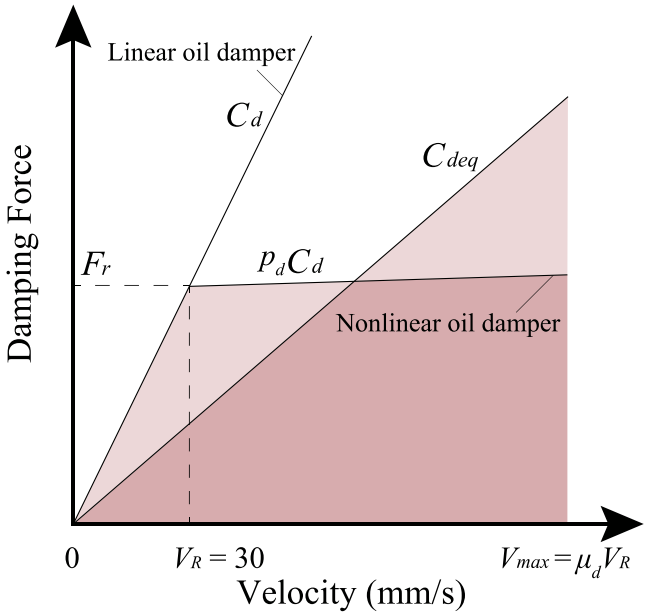

FIGURE 7 Force–Velocity relationship of nonlinear oil dampers

The seismic response of the damped braced tube system, where linear oil dampers are uniformly distributed in the slit and the corresponding viscous coefficients per oil damper are 57–294 kN·s/m, between GRSAs are compared to the responses from nonlinear response history analyses (NLRHA) as shown in Figure 8. The NLRHAs are performed by RESP[10] adopting the Newmark β method for the numerical integration, and P-delta induced geometric nonlinearity effects of members are considered. As shown in Figure 8a,c, GRSA has sufficient accuracy for investigating the seismic performance of the damped braced tube system. The first modal damping ratios of the damped braced tube where $\{\alpha, 8\{n_i\}^T\{C_{di}\}\}$ is {0.22, 20.0 MN·s/mm} and the bare slit model with the assumed achieved modal damping ratio are shown in Figure 8d. The damping ratio is calculated from the logarithmic decrement of the free vibration against one cycle sinusoidal excitation adjusted to the first mode fundamental periods. The difference of the fundamental periods is due to the dissipater element. As shown in Figure 8d, the calculated damping ratio by GRSA is accurate, and the errors of the seismic responses depend on just the modal combination method.

In this study, the "seismic performance" is assessed by parameters like fundamental periods and the damping ratios (crucial for mitigating horizontal responses—the roof displacement and acceleration to be within human tolerance limits), the story drifts (for assessing the damage to structural and non-structural members), the shear angle (which is the peak deformation angles of the panel zones composed of exterior columns, exterior beams and elastic mega braces for assessing the damage to the exterior curtain walls). Therefore, in this study, the design story drift ratio limit is set as 0.5% (such that the structural members remain elastic), and the shear angle is required to be less than 1.0% of (so that the curtain walls do not fall off.)

3 | OUTLINE OF THE PARAMETRIC STUDIES AND THE SEISMIC OPTIMIZATIONS

The corners of the exterior surfaces of the elastic mega braces are partially and vertically removed to create slits, and linear or nonlinear oil dampers are inserted in the slits. There are eight slits, and a maximum of 22 oil dampers may be distributed per slit. The depth of the slit is kept fixed and the design variables are α which is the ratio of the elevation of the slit's base to the total building height h, and the parameter $\{\{n_i\},\{C_{di}\}\}$ which is the oil damper amount per slit.

In this research, two types of distribution as shown in Figure 9 are studied to investigate the efficiency of mitigating the displacement response. The first one shown in Figure 9a is the uniform dissipater distribution where the dissipater amount per slit $\{n_i\}^T\{C_{di}\}$ is kept the same, and the response reduction effect by varying α and the total oil damper amount $8\{n_i\}^T\{C_{di}\}$ is discussed.

The second case shown in Figure 9b is the non-uniform dissipater distribution where α and the total damper amount $8\{n_i\}^T\{C_{di}\}$ are fixed, and optimal distributions of oil damper amount minimizing the seismic responses are adopted. The seismic performances of a damped braced tube system equipped with linear or nonlinear oil dampers are also studied to discuss the nonlinear effect of dissipaters.

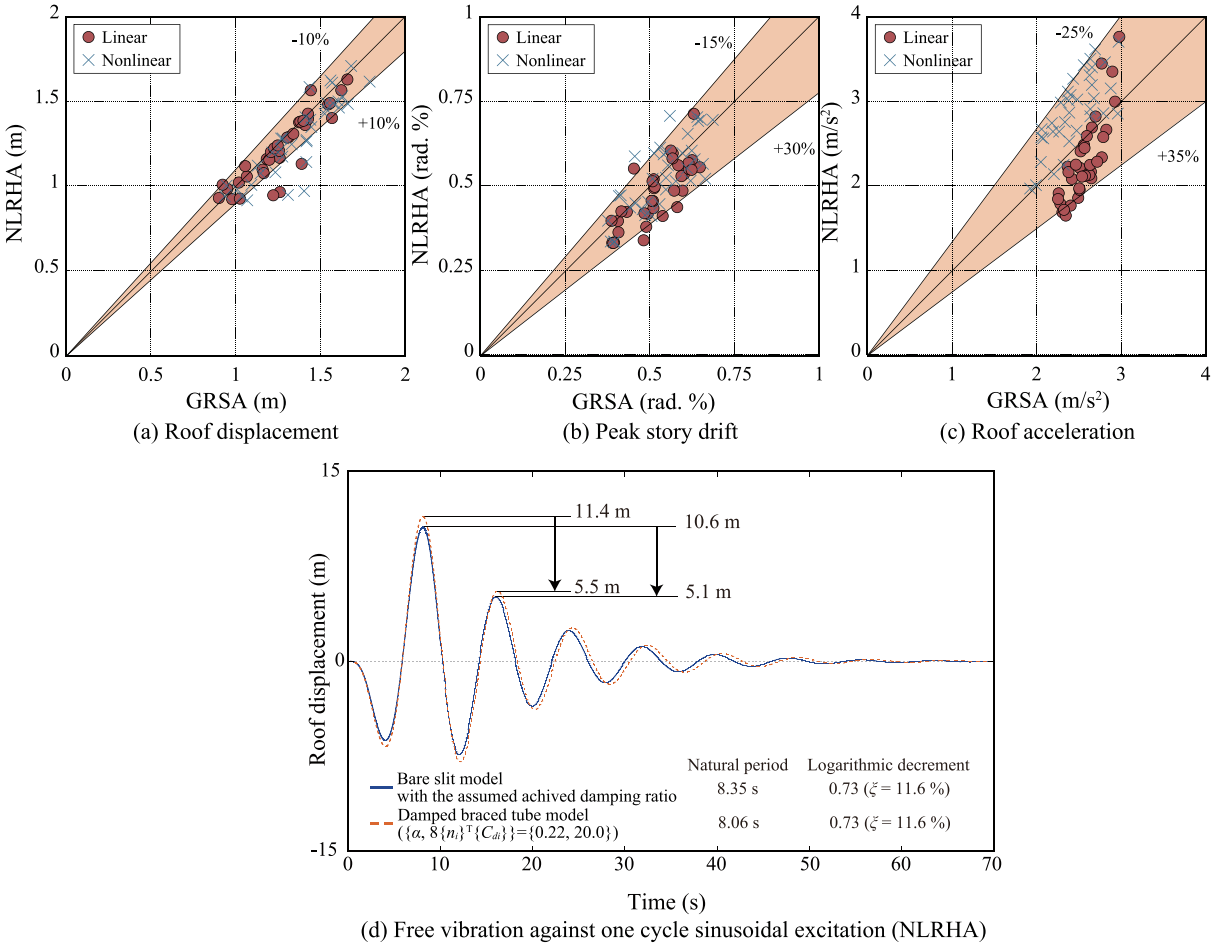

FIGURE 8 (a–d) Comparison of GRSAs and NLRHAs

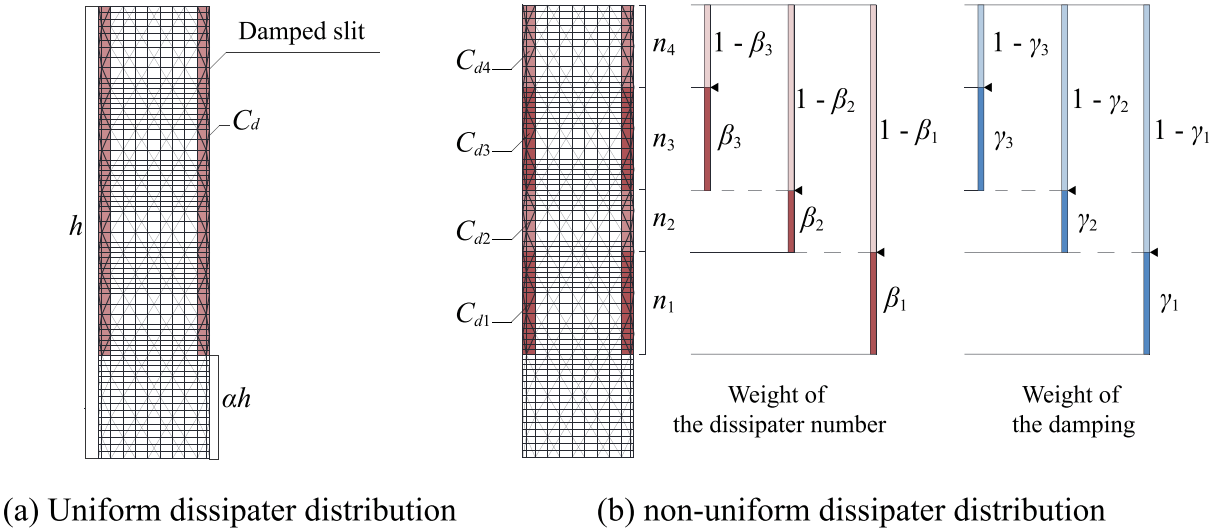

FIGURE 9 (a,b) Schematic image of the parameters to determine the distribution of the dissipater amount

As shown in Figure 9a, the dissipater amount C_d per device of the uniform dissipater distribution is calculated by Equation 4. Note that this distribution of segments is adopted for all the eight slits.

$$C_d = \{n_i\}^T \{C_{di}\}/22(1-\alpha) \tag{4}$$

The schematic image of the algorithm to determine the dissipater amount in the non-uniform dissipater distribution case is shown in Figure 9b. Here, m is the number of segments in one slit, n_i is the number of dampers in the ith segment and C_{di} is the dissipater amount per oil damper in the ith segment. n_i is expressed mathematically as function of the assigned weight β_i (Figure 9b) which represents the weight or the relative ratio of the dissipater amount of the ith segment and C_{di} may then be expressed mathematically as functions of β_i and the assigned damping weight γ_i of the dissipater amount ratio allocated to the ith segment, and the length of both vectors n_i and C_{di} depend on the total number of segments m. These parameters are calculated using Equations 5–6. For example, when the number of segment m is 3 and the total number of dissipaters per slit Σn_i is 17 (considering $\alpha = 0.22$) and the total dissipater amount per slit $\Sigma C_{di} n_i$ is 2.5 MN·s/mm (i.e., $8\{n_i\}^T\{C_{di}\} = 20.0$ MN·s/mm), the first segment's oil damper number n_1 is expressed as the weighted sum $17\beta_1$. The remaining dissipater number ratio $(1-\beta_1)$ is available for further distribution to segments 2 and 3 which is determined by the ratio β_2 and consequently, the second segment's oil damper number n_2 is expressed as $17\beta_2(1-\beta_1)$ and the third segment's oil damper number n_3 is expressed as $17(1-\beta_2)(1-\beta_1)$. Similarly, the dissipater amount per device in the ith segment C_{di} may be computed using Equation 6. The first segment's dissipater amount C_{d1} is expressed as the weighted sum $2.5\gamma_1/n_1$ MN·s/mm. The remaining dissipater number ratio $(1-\gamma_1)$ is available for further distribution to Segments 2 and 3 which is determined by the ratio γ_2, and consequently, the second segment's dissipater amount C_{d2} is expressed as $2.5\gamma_2(1-\gamma_1)/n_2$ MN·s/mm and the third segment's dissipater amount C_{d3} is expressed as $2.5(1\text{-}\gamma_2)(1\text{-}\gamma_1)/n_3$ MN·s/mm. Note that "$C_{di} = 0$ kN·s/mm" corresponds to a case where no dissipaters and no elastic mega braces are placed in the ith segment.

$$n_i = f_i(m, \{\beta_i\}) = \sum_{i=1}^{m} n_i \times \begin{cases} \beta_1 (i=1) \\ \beta_i \prod_{j=1}^{i-1} (1-\beta_j) (1<i<m) \\ \prod_{j=1}^{i-1} (1-\beta_j) (i=m) \end{cases} \tag{5}$$

$$C_{di} = g_i(m, \{\beta_j\}, \{\gamma_i\}) = \frac{\sum_{i=1}^{m} n_i C_{di}}{n_i} \times \begin{cases} \gamma_1 (i=1) \\ \gamma_i \prod_{j=1}^{i-1} (1-\gamma_j) (1<i<m) \\ \prod_{j=1}^{m-1} (1-\gamma_j) (i=m) \end{cases} \tag{6}$$

In the study of the non-uniform dissipater distribution, optimal dissipater distributions to minimize the average values of the roof displacement, the peak story drift ratio or the roof acceleration are investigated. Particle swarm optimization (PSO) distributed by Python Module DEAP[20] is adopted as the optimization algorithm, and the PSO parameters are summarized in Table 1. The optimization problems are defined as follows,

TABLE 1 Optimization specification of the non-uniform dissipater distribution

Optimize	**Damper size distribution (fixed layout)**		
Optimization algorithm	Particle Swarm Optimization (PSO)		
Minimize	Mean of roof displacements	Mean of peak story drifts	Mean of roof accelerations
Design variables	β_i: Weight of the dissipater number in the ith segment ($0 \leqq \beta_i \leqq 1$, $1 \leqq i \leqq m-1$) γ_i: Weight of the damping in the ith segment ($0 \leqq \gamma_i \leqq 1$, $1 \leqq i \leqq m-1$)		
The number of design variables	$2m-2$		
Subject to	m: The number of divisions in one slit ($1 \leqq m \leqq 5$) α: Ratio of the elevation of the slit's base to the total building height ($\alpha = 0.22$) $8\{n_i\}^T\{C_{di}\}$: The total capacity of dissipaters ($8\{n_i\}^T\{C_{di}\} = 20$ MN·s/mm)		
Inertia w used in PSO	1.0		
Personal best priority c_1 used in PSO	2.0		
Global best priority c_2 used in PSO	2.0		

$$Optimize\ \{\{n_i\},\{C_{di}\}\} = \{\{f_i(m,\beta_i)\},\{g_i(m,\beta_i,\gamma_i)\}\} \tag{7}$$

$$Minimize\ p(\{\{n_i\},\{C_{di}\}\}) = p(\boldsymbol{x}) = \frac{1}{k}\sum_{i=1}^{k} R_{CQC}^{\text{Roof displacement}}{}_i, \frac{1}{k}\sum_{i=1}^{k} R_{CQC}^{\text{Peak story drift}}{}_i \text{ or } \frac{1}{k}\sum_{i=1}^{k} R_{CQC}^{\text{Roof acceleration}}{}_i \tag{8}$$

$$Subject\ to\ Fixed\left\{\alpha, m, 8\{n_i\}^T\{C_{di}\}\right\}, 0.0 \le \beta_i \le 1.0\ ,\ \ 0.0 \le \gamma_i \le 1.0 \tag{9}$$

$$Variable\ \boldsymbol{x} = \{\{\beta_1,\ldots,\beta_i,\ldots,\beta_{m-1}\},\{\gamma_1,\ldots,\gamma_i,\ldots,\gamma_{m-1}\}\}(i = 1,2,\ldots m) \tag{10}$$

where k is the number of the seismic waves equal to 4 for the spectrally matched waves and 1 for the KA1 wave.

4 | SEISMIC PERFORMANCE OF DAMPED BRACE TUBE SYSTEM INCORPORATING LINEAR OIL DAMPERS

The seismic performance of the damped braced tube system with linear oil dampers is discussed in this section. As shown in Figure 7, even nonlinear oil damper demonstrates the same damping performance (the fundamental period and the damping ratios) within lower than the relief velocity of the device. Therefore, the damping performance discussed here also corresponds to the performance against wind load and SLE level earthquake though the seismic inputs in this study are DBE level.

4.1 | Uniform dissipater distribution model

The contour maps of the modal characteristics of the uniform dissipater distribution models where the same dissipater amount is distributed in each dissipater brace are shown in Figure 10. In the contour map, the vertical axis is the height ratio α, and the horizontal axis is the total dissipater amount $8\{n_i\}^T\{C_{di}\}$. As discussed before in Section 3, $\{\alpha, 8\{n_i\}^T\{C_{di}\}\} = \{1.0, 0.0\}$ corresponds to the performance of a "No damper" model. Note that the fundamental periods shown in the contour map were calculated considering non-proportional damping. The sections of the contour map with fixed α or $8\{n_i\}^T\{C_{di}\}$ are shown in Figure 10b1–b3,d1–d3. As shown in Figure 10a1–a3, the fundamental periods (especially the 1st modal fundamental period) are longer for deeper damper slits and shorter for larger total dissipater capacities. As shown in Figure 10c1–c3, the shortest fundamental period is that of the no damper model. As shown in Figure 10b1–b3,d1–d2, the modal damping ratios increase with the depth of the slit, while an optimal value exists for the total dissipater amount. According to the complex eigenvalue analysis results in the author's previous study,[9,21–23] the damped outrigger system was found to be the most effective in increasing only the first-order mode damping ratio. Compared to this result, it is a noteworthy advantage of the damped braced tube system with the damping ratios of the second and third modes higher than 7%. However, there is a trade-off between the fundamental periods and the modal damping ratios. For example, if α is too large, only a marginal increase in the damping ratio is obtained, and if α is too small, the fundamental periods becomes too long, which suggests that it is crucial to balance the fundamental periods and the modal damping ratios while designing the damped braced tube system. Based on the analysis results, a design value of 0.22 is recommended for α.

The contour maps of the average values of the roof displacement or the peak story drift ratio for the different seismic inputs are shown in Figure 11. As shown in Figure 11a1–a4, the roof displacement and the peak story drift ratio reduce with the depth of the slit. The seismic response against the spectrally matched waves with a considerable higher mode response is larger than that from the artificial KA1 wave. As shown in Figure 11b3–b4, the seismic response reduction effect against KA1 waves, where the first mode response is excited will be improved if the total dissipater amount is increased to obtain shorter the first mode fundamental period even though the first mode damping ratio is slightly reduced. In contrast, the seismic responses against the spectrally matched waves are higher when the total dissipater amount is large. This is due to the higher mode excitation from the resulting short fundamental periods when the dissipater amount is large, as shown in the acceleration response spectra in Figure 6. The shear angles shown in Figure 11c,d are the peak deformation angles of the panel zones composed of exterior columns, exterior beams and elastic mega braces, and are used as damage indicators for the exterior curtain walls. A shear angle of 0.01 rad. is the design limit criteria for curtain walls allowing ceiling damage but not collapse as per the Japanese standard.

Based on the results of the uniform dissipater distribution models, $\{\alpha, 8\{n_i\}^T\{C_{di}\}\}$ is fixed at {0.22, 20 MN·s/mm} in the subsequent non-uniform dissipater distribution models. These values were selected to achieve a first mode damping ratio of more than 10%, a first mode fundamental period and a peak story drift ratio of less than 0.5% rad while assuming a realistic total dissipater amount considering the standard viscous damping devices available in Japan. Particularly for the ratio α of the slit base height to the building height, 0.0 is best for the obtained damping ratio but actually make it difficult to design foundation against the over turning moment and then 0.22 is practical. α is also fixed at about 0.22 in

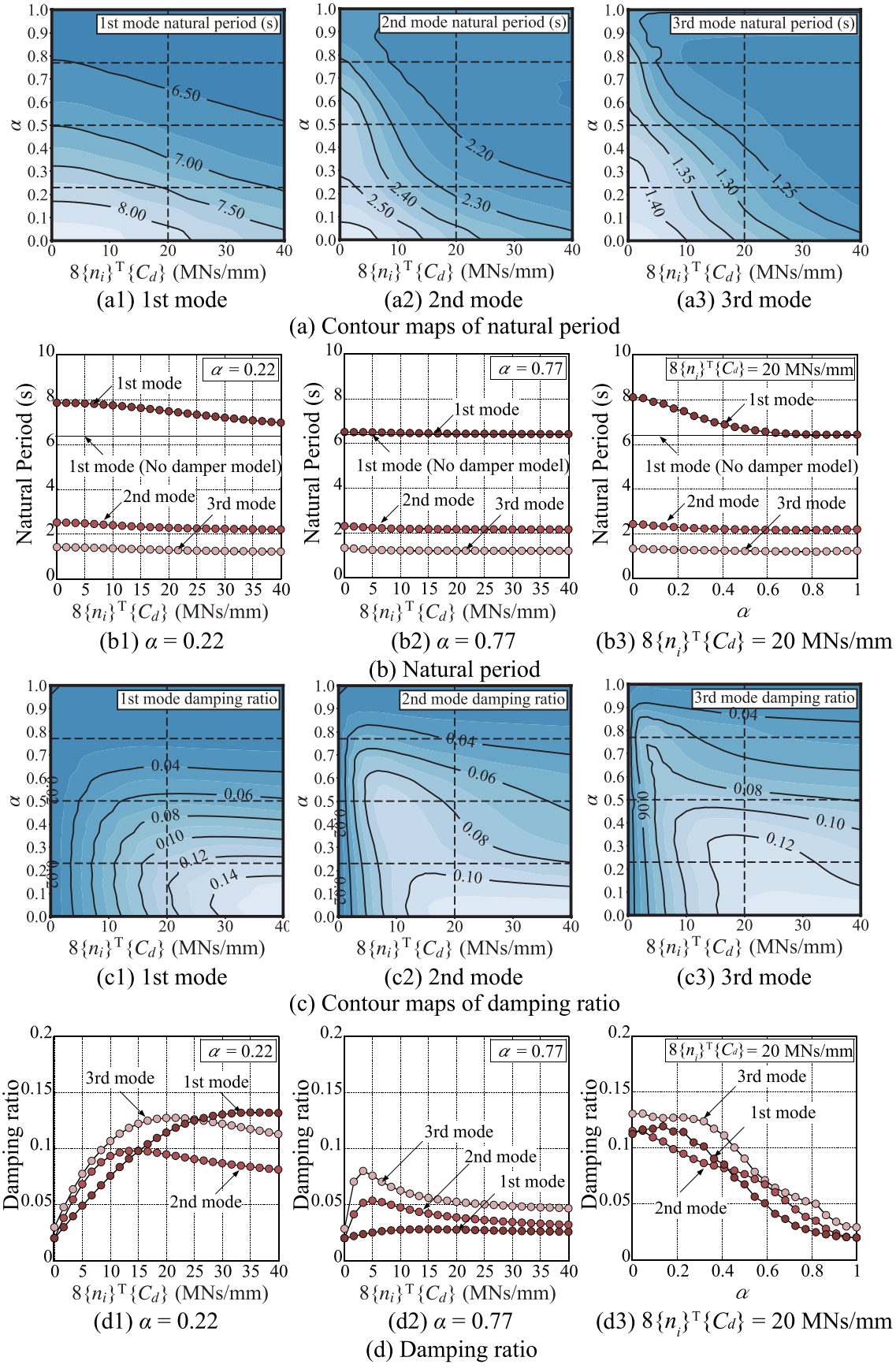

FIGURE 10 (a–d) Modal characteristics of the uniform dissipater distribution models with linear oil dampers

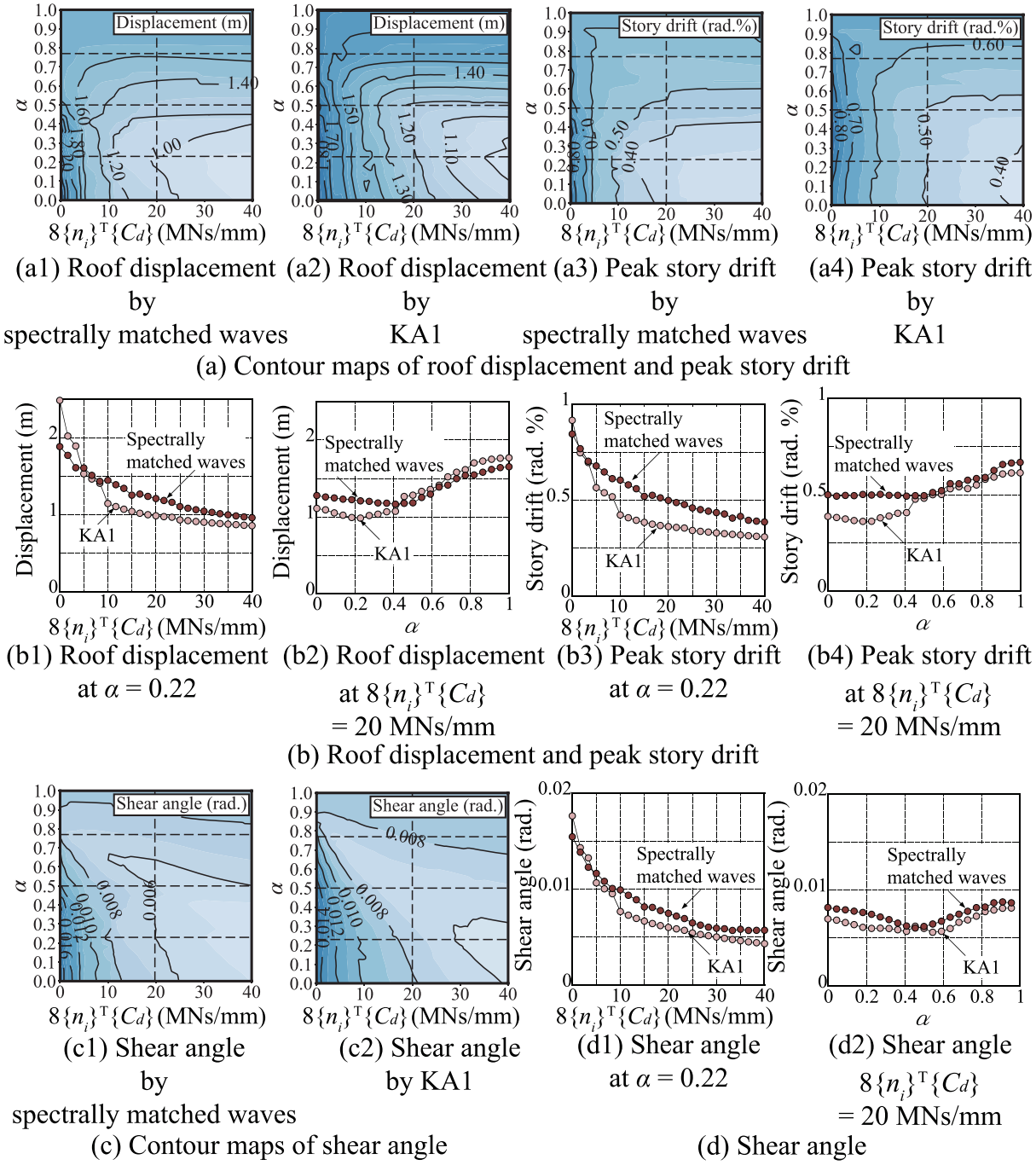

FIGURE 11 (a–d) Contour maps of the average seismic responses for the uniform dissipater distribution models with linear oil dampers

the actual project based on this result. As shown in Figures 10 and 11, throughout the range of modal damping ratios, the story drift ratios are within 0.5% rad. While the main frame members remain elastic, the shear angles are within 1.0% rad, and the curtain walls do not fall off. This suggests that the damped braced tube system provides a wide range of design options for the depth of the slit and the total dissipater amount.

4.2 | Non-uniform dissipater distribution model

The optimal distribution of the linear oil damper amount and the seismic responses of the non-uniform dissipater distribution models are shown in Figure 12. The optimal distribution of the dissipater amount depends on the specific seismic response to be minimized and the seismic input, which is in agreement with the author's previous seismic optimization results. In the obtained optimal distribution, a larger dissipater amount is

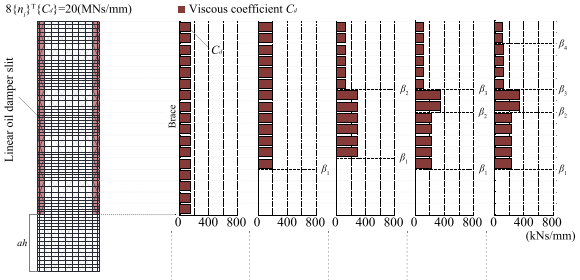

Number of segments	1	2	3	4	5
Roof displacement (m)	1.207	1.192	1.183	1.182	1.182
Peak story drift (rad.%)	0.499	0.485	0.501	0.503	0.501
Roof acceleration (m/s²)	2.531	2.601	2.610	2.600	2.615
1st mode damping ratio (%)	11.4	11.1	11.6	11.8	11.9

(a1) Minimization of roof displacement by spectrally matched waves

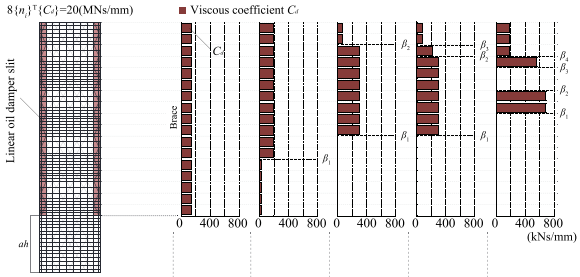

Number of segments	1	2	3	4	5
Roof displacement (m)	1.207	1.120	1.201	1.207	1.232
Peak story drift (rad.%)	0.499	0.484	0.466	0.460	0.450
Roof acceleration (m/s²)	2.531	2.568	2.582	2.682	2.132
1st mode damping ratio (%)	11.4	11.0	11.2	10.4	9.4

(b1) Minimization of peak story drift by spectrally matched waves

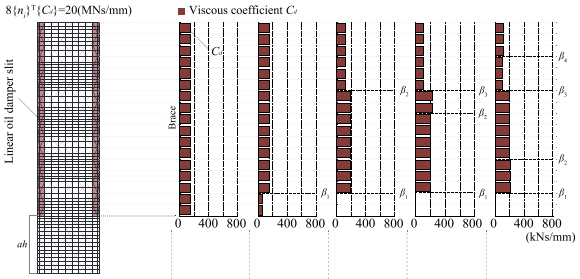

Number of segments	1	2	3	4	5
Roof displacement (m)	0.983	0.981	0.979	0.979	0.979
Peak story drift (rad.%)	0.362	0.361	0.355	0.352	0.354
Roof acceleration (m/s²)	1.042	1.051	1.058	1.062	1.056
1st mode damping ratio (%)	11.4	11.5	11.9	12.0	12.0

(a2) Minimization of roof displacement by KA1

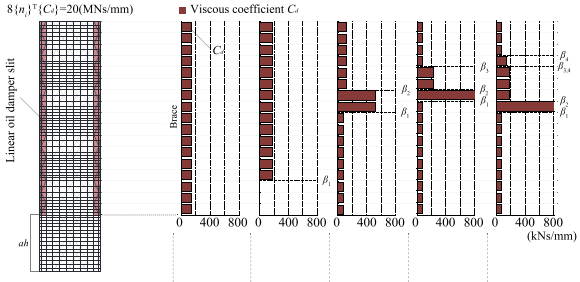

Number of segments	1	2	3	4	5
Roof displacement (m)	0.983	0.987	0.992	0.998	0.997
Peak story drift (rad.%)	0.362	0.356	0.340	0.337	0.332
Roof acceleration (m/s²)	1.042	1.112	1.092	1.146	1.077
1st mode damping ratio (%)	11.4	11.8	11.3	11.4	11.2

(b2) Minimization of peak story drift by KA1

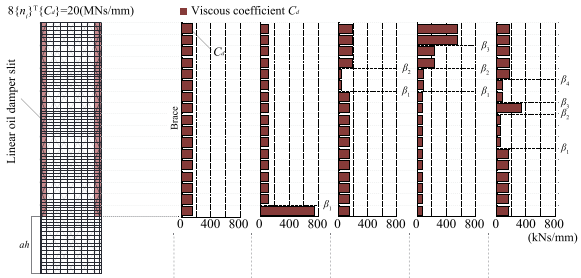

Number of segments	1	2	3	4	5
Roof displacement (m)	1.207	1.247	1.212	1.305	1.218
Peak story drift (rad.%)	0.499	0.524	0.492	0.537	0.495
Roof acceleration (m/s²)	2.531	2.085	2.077	2.072	2.067
1st mode damping ratio (%)	11.4	10.9	11.2	8.21	11.1

(c1) Minimization of roof acceleration by spectrally matched waves

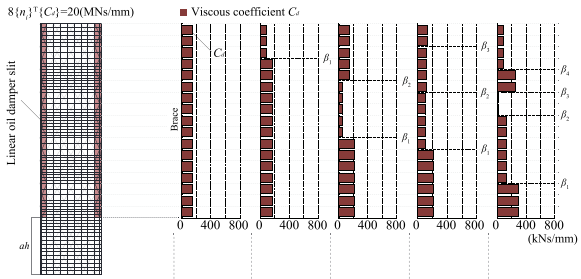

Number of segments	1	2	3	4	5
Roof displacement (m)	0.983	0.983	1.000	0.992	1.000
Peak story drift (rad.%)	0.362	0.358	0.376	0.369	0.375
Roof acceleration (m/s²)	1.042	1.021	0.986	0.982	0.910
1st mode damping ratio (%)	11.4	11.7	11.0	11.2	11.1

(c2) Minimization of roof acceleration by KA1

FIGURE 12 (a1–c2) Optimal distribution of the linear oil dampers and the seismic responses of the non-uniform dissipater distribution models

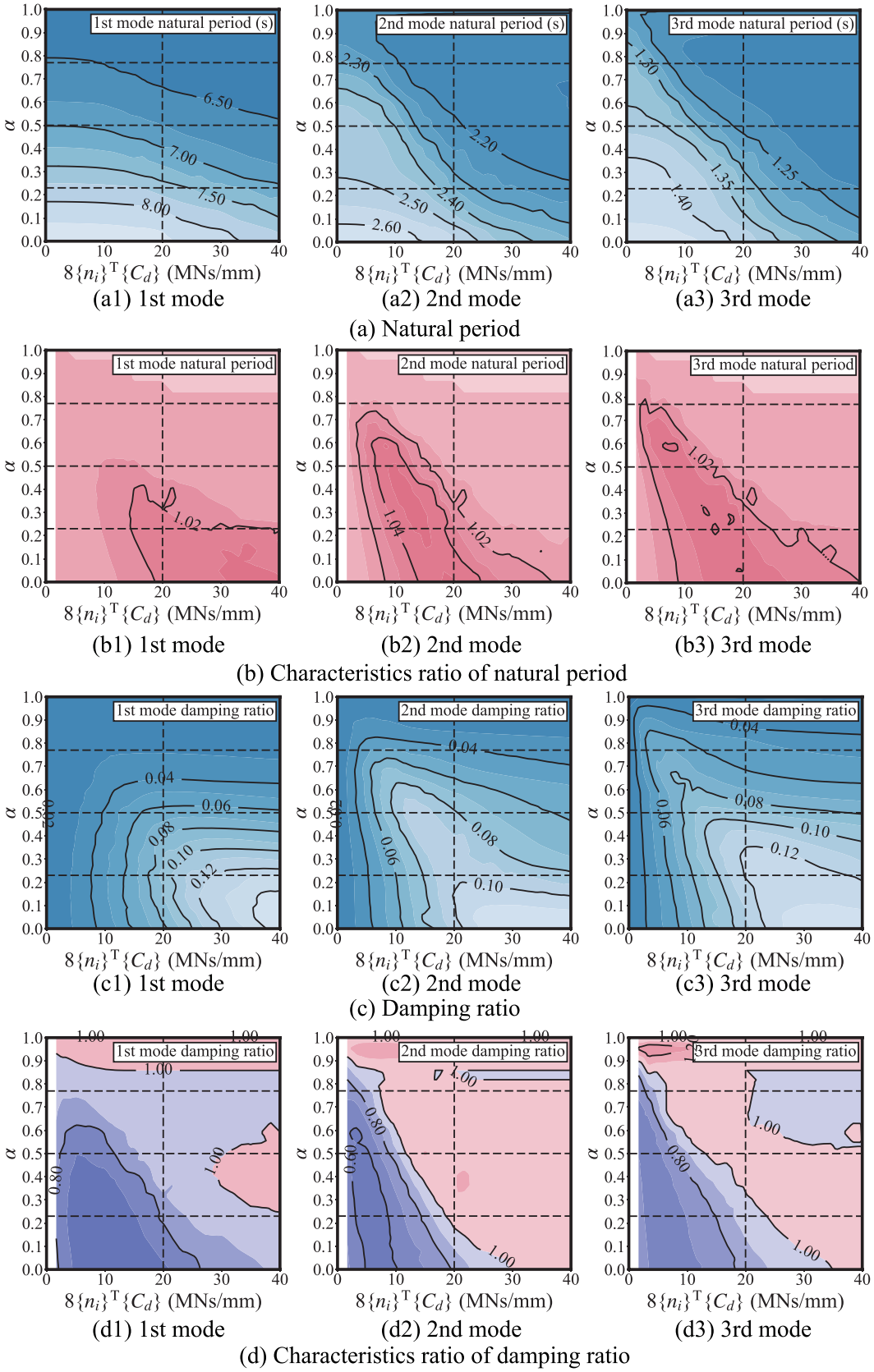

FIGURE 13 (a–d) Modal characteristics of the uniform dissipater distribution models with nonlinear oil dampers

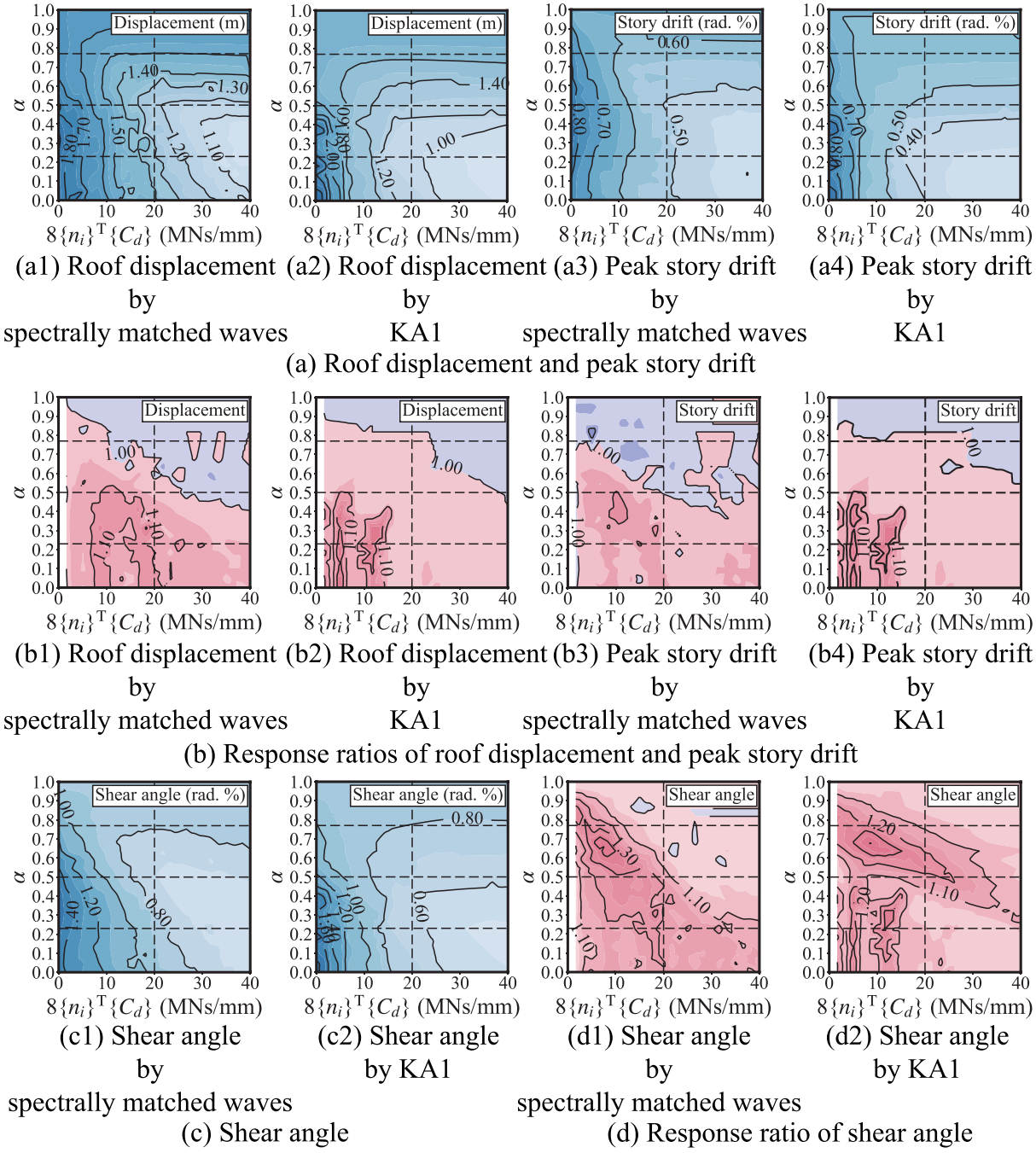

FIGURE 14 (a–d) Contour maps of the seismic responses and response ratios of the models with the nonlinear oil dampers to the model with the linear oil dampers

distributed in the lower segments for minimizing the roof displacement, while a small dissipater amount is distributed to the middle to upper segments for minimizing the peak story drift ratio. The differences in the optimal distribution of the linear oil damper amount obtained for the different seismic waves may be attributed to the excitation of the higher mode responses. For example, a distribution similar to the uniform distribution is selected to minimize the roof acceleration against the KA1 wave that primarily excites the first mode response, while a larger dissipater amount is distributed in the upper segment against the spectrally matched waves that excite even the higher mode responses. Increasing segments (larger m) may reduce the seismic responses, but the cost of dissipaters increases. However, regardless of the seismic response parameter being minimized or the number of the segments, the story drift ratios for all the optimal cases are within 0.5% rad, when the main frame members remain elastic. Furthermore, as shown in Figure 12b1, the discontinuous dissipater distribution where the dissipater is not distributed in all parts of the slit gives similar effects, providing an efficient design alternative.

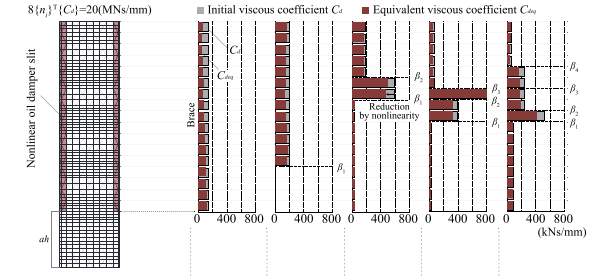

Number of segments	1	2	3	4	5
$8\{n_j\}^T\{C_{deq}\}$ (MNs/mm)	14.09	15.35	15.15	14.83	14.49
Roof displacement (m)	1.302	1.274	1.242	1.228	1.221
Peak story drift (rad.%)	0.519	0.495	0.520	0.518	0.486
Roof acceleration (m/s²)	2.411	2.311	2.413	2.543	2.424
1st mode damping ratio (%)	9.4	10.0	9.5	9.8	10.4

(a1) Minimization of roof displacement by spectrally matched waves

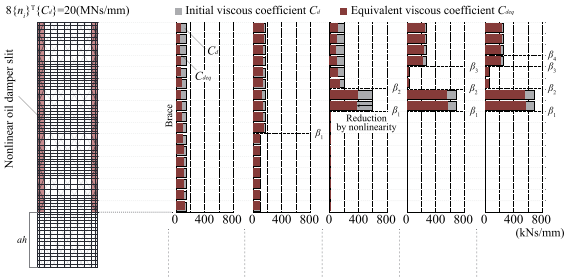

Number of segments	1	2	3	4	5
$8\{n_j\}^T\{C_{deq}\}$ (MNs/mm)	14.09	15.08	14.35	15.53	15.64
Roof displacement (m)	1.302	1.259	1.355	1.300	1.262
Peak story drift (rad.%)	0.519	0.493	0.477	0.472	0.464
Roof acceleration (m/s²)	2.411	2.326	2.420	2.397	2.425
1st mode damping ratio (%)	9.4	9.7	9.2	8.9	9.0

(b1) Minimization of peak story drift by spectrally matched waves

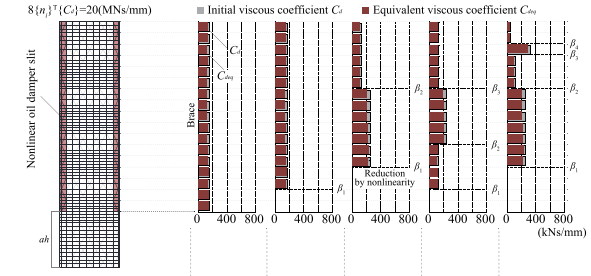

Number of segments	1	2	3	4	5
$8\{n_j\}^T\{C_{deq}\}$ (MNs/mm)	17.50	17.38	17.22	17.26	17.20
Roof displacement (m)	1.009	1.001	0.999	0.998	0.997
Peak story drift (rad.%)	0.372	0.368	0.359	0.360	0.359
Roof acceleration (m/s²)	1.273	1.287	1.302	1.294	1.307
1st mode damping ratio (%)	10.5	10.8	11.2	11.0	11.2

(a2) Minimization of roof displacement by KA1

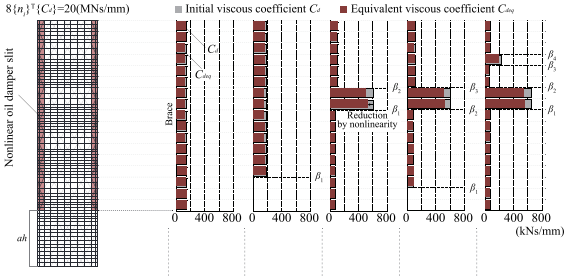

Number of segments	1	2	3	4	5
$8\{n_j\}^T\{C_{deq}\}$ (MNs/mm)	17.50	17.41	17.37	17.34	17.35
Roof displacement (m)	1.009	1.001	1.008	1.006	1.009
Peak story drift (rad.%)	0.372	0.368	0.344	0.343	0.341
Roof acceleration (m/s²)	1.273	1.297	1.329	1.336	1.336
1st mode damping ratio (%)	10.5	10.7	10.7	10.8	10.8

(b2) Minimization of peak story drift by KA1

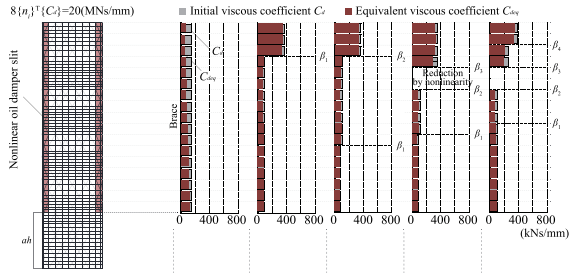

Number of segments	1	2	3	4	5
$8\{n_j\}^T\{C_{deq}\}$ (MNs/mm)	14.09	15.16	15.10	15.02	15.17
Roof displacement (m)	1.302	1.342	1.335	1.334	1.341
Peak story drift (rad.%)	0.519	0.538	0.533	0.534	0.537
Roof acceleration (m/s²)	2.411	2.246	2.236	2.236	2.235
1st mode damping ratio (%)	9.4	8.34	8.43	8.46	8.44

(c1) Minimization of roof acceleration by spectrally matched waves

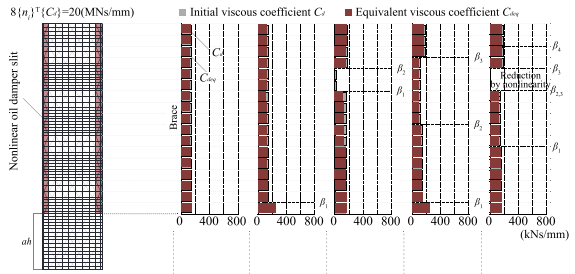

Number of segments	1	2	3	4	5
$8\{n_j\}^T\{C_{deq}\}$ (MNs/mm)	17.50	17.54	17.53	17.60	17.60
Roof displacement (m)	1.009	1.013	1.012	1.016	1.014
Peak story drift (rad.%)	0.372	0.374	0.374	0.378	0.376
Roof acceleration (m/s²)	1.273	1.271	1.270	1.269	1.267
1st mode damping ratio (%)	10.5	10.5	10.5	10.3	10.4

(c2) Minimization of roof acceleration by KA1

FIGURE 15 (a1–c2) Optimal distributions of nonlinear oil dampers and the seismic response of the optimized models

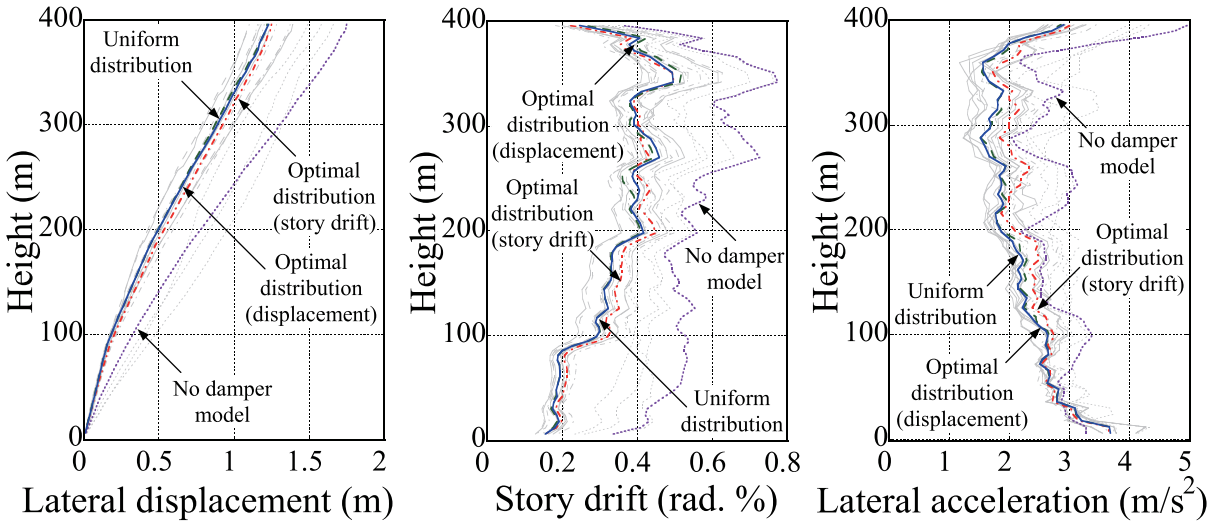

FIGURE 16 NLRHA results of optimal dissipater design solutions

5 | SEISMIC PERFORMANCE OF THE DAMPED BRACE TUBE SYSTEM INCORPORATING NONLINEAR OIL DAMPERS

This section discusses the seismic performance of the damped braced tube system with nonlinear oil dampers.

5.1 | Uniform dissipater distribution model

The contour maps of the modal characteristics of the uniform dissipater distribution models where the same dissipater amount is distributed in every nonlinear oil damper brace slit are shown in Figure 13. The characteristic ratios of the models with nonlinear oil dampers to the models with linear oil dampers are shown in Figure 13b,d. Note that while the initial distribution of viscous coefficient is uniform along the damped slit, the final distribution of the equivalent viscous coefficient considering nonlinearity of oil dampers is non-uniform depending on both the kind of the seismic waves and the seismic responses. Under large earthquakes, the equivalent periods become longer than the initial periods due to the nonlinearity of the dissipater (secant stiffness), and the modal damping ratios decrease compared to the initial performance. For example, as shown in Figure 13b,d, the performance of the model with $\{\alpha, 8\{n_i\}^T\{C_{di}\}\} = \{0.22, 20\ \text{MN·s/mm}\}$ against the large earthquake of $S_v = 80$ cm/s results in the first mode fundamental period about 2% longer and the first mode damping ratio about 20% lower from the initial performance. If a similar nonlinear damping performance to the initial performance is desired even in the large earthquakes, a larger dissipater amount is required. Regardless, the damped braced tube system provides around 10% first- to third-modal damping ratio even under a large earthquake.

The contour maps of the seismic responses and the response ratios of the models with the nonlinear oil dampers to the model with the linear oil dampers are shown in Figure 14. As shown in Figure 14a1–a4, the seismic responses are higher for nonlinear oil dampers. The main frame may be damaged when the total initial viscous coefficient falls below 5 MN·s/mm. As shown in Figure 14b1–b4, even with the nonlinear oil dampers with $\{\alpha, 8\{n_i\}^T\{C_{di}\}\} = \{0.22, 20\ \text{MN·s/mm}\}$, the response may be reasonably controlled by keeping the story drift ratio under 0.5% rad. Even against the large earthquake with $S_v = 80$ cm/s. These results indicate that the seismic performance of the proposed damped brace tube system satisfies all the Japanese seismic code requirements.

5.2 | Non-uniform dissipater distribution model

The obtained optimal distribution of nonlinear oil dampers and the seismic response of the optimized models are shown in Figure 15. In Figure 15, both the distribution of the initial and the equivalent viscous coefficient are described together; the larger differences between C_{deq} and C_d indicate the effect of nonlinearity of the dissipaters. As shown in Figure 15a2–b2, the total equivalent viscous coefficient $8\{n_i\}^T\{C_{deqi}\}$ of the nonlinear oil dampers against the spectrally matched waves reduce to 20% to 30% of the total initial viscous coefficient $8\{n_i\}^T\{C_{di}\}$, and few of the optimal distributions of the nonlinear oil damper amount are different from those obtained for the linear oil damper cases. However, the seismic responses of the optimized non-uniform dissipater distribution models with the nonlinear oil dampers significantly reduce the peak story drift

ratio response and the peak drifts are within 0.5% rad. Based on the results and the discussions in Sections 4 and 5, it may be concluded that the optimal dissipater distribution depends on both dissipater type (linear or nonlinear) and the specific seismic input (the spectrally matched waves exciting higher modes or the long period wave exciting only first mode), and it is suggested to select a dissipater distribution considering both the target design earthquakes and the dissipater types. Furthermore, as shown in Figures 12 and 15, there is a trade-off between the minimized displacement-based responses and the minimized acceleration responses, but the differences between the minimized responses and the non-minimized responses are not so big for the damped braced tube system with an appropriate total dissipater amount. Therefore, it is concluded that minor changes in damper distribution does not significantly influence the overall seismic performance, which provides flexibility in design with respect to the dissipater distributions.

The NLRHA results of the five segmented damped braced tube models with the nonlinear oil dampers are shown in Figure 16. The colored line shows the mean responses of the damped models and the peak responses of the "No damper model." While all the cases reduce the peak responses to 50% of the "No damper model," all of the different distribution options provide similar seismic response reduction effects. This indicates that the damped braced tube system provides a wide range of dissipater distributions and even permits concentration of dissipaters to limited segments.

6 | CONCLUSION

This paper proposed a novel damped braced tube system for tall buildings in seismic areas, where the exterior surface of the elastic mega braces are partially and vertically removed and dissipaters are inserted in the vertical slits. According to the vast parametric studies and the seismic optimizations, the following results are obtained.

1. The proposed damped braced tube system was employed on a supertall building model (based on a real project) with a 97 $\times$ 97 m plan and height of 397 m. The damped system provided damping ratios of around 7% for the first three modes and the seismic response against the Japanese Level-2 earthquakes ($S_v = 80$ cm/s) was reduced to about 50% of the response of a conventional braced tube system. Considering the trade-off between the first modal damping ratio and the fundamental period, the elevation of the slit's base is recommended to be equal to 0.22 of the total building height ($\alpha = 0.22$).
2. The total dissipater amount significantly influences the seismic performance of the damped braced tube system, and the seismic response significantly reduces keeping the main frame undamaged if a modal damping ratio of 7.0% or more is obtained. While there is a trade-off relationship between the minimized displacement-based responses and the minimized acceleration responses, the differences between the minimized responses and the non-minimized responses are not so big if sufficient total dissipater amount is employed. Thus, the seismic performance is not highly sensitive to the damper distribution, which allows for flexibility in design with respect to the dissipater distributions.
3. The damping performance of a damped braced tube system incorporating nonlinear oil dampers was found to deteriorate from the initial performance of system with linear dampers as the seismic response increased. The seismic responses of an appropriately designed damped braced tube (e.g., considering a ratio of 0.22 between the slit base elevation to the building height and a total dissipater amount 20 MN·s/mm against the Japanese Level-2 earthquakes [i.e. DBE level]) increased by around 10% if compared to the seismic responses of the system incorporating linear oil dampers. As the optimal dissipater distribution depends on both the dissipater type (linear or nonlinear oil dampers) and the specific seismic inputs (the spectrally matched waves exciting higher mode response or the long period earthquake exciting only first mode), it is recommended to select a dissipater distribution considering both the target design earthquakes and the dissipater types. A good design where the depth of the slit and the distribution of the dissipaters are such that sufficient initial damping is achieved allowed the nonlinear seismic responses to remain in a range that prevents the main frame from damage.

The future scope of this work includes expansion of the damped braced tube system to include other types of dissipaters (i.e., fluid viscous damper, friction damper, or an elasto-plastic damper), applying the damped slits to the center of the exterior surfaces, or investigating the effect of the number of consecutive stories that the braces connect.

ACKNOWLEDGMENTS

This work was supported by a research fund by the Japanese Society of Seismic Isolation (JSSI) and by a Grant-in-Aid from the Japan Society for the Promotion of Science Fellowships (No. 21K14288). A campus supercomputer (TSUBAME 3.0 at the Tokyo Institute of Technology) was used to perform the analyses for the optimization study. The authors also appreciate the proof reading by Deepshikha Nair from Tokyo Institute of Technology.

AUTHOR STATEMENT

Yoji Ishibashi: Conceptualization, Writing – review. **Yuki Terazawa**: Supervision, Conceptualization, Methodology, Investigation, Formal analysis, Writing – original draft, Writing – review & editing. **Haruki Tanaka**: Investigation. **Ryo Yokoyama**: Conceptualization, Investigation. **Hiroki Mizuno**: Conceptualization. **Toru Takeuchi**: Supervision, Writing – review.

DATA AVAILABILITY STATEMENT

The data that support the findings of this study are available from the corresponding author upon reasonable request.

ORCID

Yuki Terazawa https://orcid.org/0000-0003-4808-1885
Toru Takeuchi https://orcid.org/0000-0001-7430-4734

REFERENCES

[1] A. Lago, T. Trabucco, A. Wood, *Damping Technologies for Tall Buildings Theory, Design, Guidance and Case Studies*, Vol. 9, Council on Tall Buildings and Urban Habitat, Elsiver Inc.Amsterdam, Netherlands **2018**.
[2] Tokyo Torch Market. https://www.mec.co.jp/tokiwabashi/
[3] R. J. Smith, M. R. Willford, *Struct. Design Tall Spec. Build.* **2007**, *16*(501–517), 11.
[4] B. S. Smith, A. Coull, Chapter 14, in *Tall Building Structures Analysis and Design*, John Wiley & Sons, Inc.Toronto, Canada **1991**.
[5] H. Bin, T. Takeuchi, *Earthquake Spectra*, vol. *33*, no. 2, pp. 665–685, **2017**.5
[6] P.-C. Lin, T. Takeuchi, R. Matsui, *Earthq. Eng. Struct. Dyn.* **2018**, *47*, 2343.
[7] P. Tan, C. J. Fang, W. R. Tu, F. L. Zhou, Y. Wang, M. Jiang, Experimental study on the outrigger damping system for high-rise building. *Proceedings of the 15th World Conference on Earthquake Engineering*, Lisbon, Portugal, **2012**.
[8] M. Morales-Beltran, G. Turan, O. Dursun, R. Nijsse, *Struct. Design Tall Spec. Build.* **2019**, *28*, e1554.
[9] P.-C. Lin, T. Takeuchi, *Jpn. Archit. Rev.* **2019**, *2*(10), 392.
[10] RESP-D. https://www4.kke.co.jp/resp/
[11] I. Almufti, J. Krolicki, A. Chrowter, The resilience-based design of the 181 Fremont tower. *Structure Magazine* **2016**, *6*, 42.
[12] Ministry of Construction, Japan. Ministerial Notification No. 1457 of the Ministry of Construction, Japan, **2000**. (in Japanese)
[13] Bureau of the Ministry of Land, Infrastructure, Transport and Tourism. Technical Advice No. 1111 from the Director of the Housing Bureau of the Ministry of Land, Infrastructure, Transport and Tourism, **2016** (in Japanese)
[14] The Ministry of Construction. Commentary of the technical background about the regulations of the revised Japanese Building Law, Gyousei, **2001**. (in Japanese)
[15] Y. Terazawa, T. Takeuchi, *Earthquake Spectra* **2018**, *34*(3), 1459.
[16] Y. Terazawa, T. Takeuchi, *Jpn Archit Rev.* **2019**, *2*, 477.
[17] Y. Terazawa, W. Sano, T. Takeuchi, *J. Struct. Constr. Eng. Trans. AIJ* **2020**, *85*(775), 1187. (in Japanese)
[18] R. Sinha, T. Igusa, *Earthq. Eng. Struct. Dyn.* **1995**, *24*, 615.
[19] Japan Society of Seismic Isolation (JSSI), *Manual for design and construction of passively-controlled buildings*, 3rd ed., Daioh Co., Ltd., Japan **2013**.
[20] DEAP. DEAP 1.1.0 https://github.com/DEAP/deap
[21] Y. Terazawa, T. Asai, S. Ishibashi, T. Takeuchi, *J. Struct. Constr. Eng. Trans. of AIJ* **2020**, *85*(774), 1067. (in Japanese)
[22] Y. Terazawa, S. Ishibashi, H. Omura, T. Asai, T. Takeuchi, *J. Struct. Constr. Eng. Trans. of AIJ* **2022**, *87*(791), 149. (in Japanese)
[23] T. Asai, T. Terazawa, T. Miyazaki, P. C. Lin, T. Takeuchi, *Eng. Struct.* **2021**, *247*(11), 113229.

How to cite this article: Y. Ishibashi, Y. Terazawa, H. Tanaka, R. Yokoyama, H. Mizuno, T. Takeuchi, *Struct Design Tall Spec Build* **2022**, e1926. https://doi.org/10.1002/tal.1926